NMR Structure of a Complex Formed by the Carboxyl-Terminal Domain of Human RAP74 and a Phosphorylated Peptide from the Central Domain of the FCP1 Phosphatase[†,‡]

Ao Yang,[§] Karen L. Abbott,[||] Alexandre Desjardins,[§] Paola Di Lello,[§] James G. Omichinski,*[,§] and Pascale Legault*[,§]

Département de Biochimie, Université de Montréal, C.P. 6128, Succursale Centre-Ville, Montréal, QC, Canada H3C 3J7, and Department of Biochemistry and Molecular Biology, University of Georgia, Athens, Georgia 30602

Received August 15, 2008; Revised Manuscript Received December 4, 2008

ABSTRACT: Recycling of RNA polymerase II (RNAPII) requires dephosphorylation of the C-terminal domain (CTD) of the largest subunit of the polymerase. FCP1 enables the recycling of RNAPII via its CTD-specific phosphatase activity, which is stimulated by the RAP74 subunit of the general transcription factor TFIIF. Both the central (centFCP1) and C-terminal (cterFCP1) domains of FCP1 interact independently and specifically with the C-terminal domain of RAP74 (cterRAP74), suggesting that these interactions mediate the stimulatory effect of TFIIF on the CTD phosphatase activity of FCP1. Phosphorylation of FCP1 by casein kinase 2 on residues in its central (T584) and C-terminal (S942 and S944) domains stimulates its binding to RAP74 and its CTD phosphatase activity. To improve our understanding of the FCP1−RAP74 interactions, we previously determined the NMR structure of a complex formed by human cterRAP74 and cterFCP1. We now present the high-resolution NMR structure and thermodynamic characterization by isothermal titration calorimetry of a complex formed by the same cterRAP74 domain and a phosphorylated peptide from the central domain of human FCP1 (centFCP1-PO_4). Comparison of the cterFCP1−cterRAP74 and centFCP1-PO_4−cterRAP74 complexes indicates that centFCP1 and cterFCP1 both utilize hydrophobic and acidic residues to recognize the same groove of RAP74, but there are significant differences in the details of their interactions. These differences point to the adaptability of RAP74 to recognize the two regions of FCP1. Our NMR and thermodynamic studies further elucidate the complex molecular mechanism by which TFIIF and FCP1 cooperate for RNAPII recycling.

The carboxyl-terminal domain (CTD)[1] of RNA polymerase II (RNAPII) plays a pivotal role in regulating gene expression in eukaryotes. The CTD not only controls the cycle of mRNA transcription but also allows for efficient coupling between mRNA transcription and cotranscriptional processes, such as mRNA capping and processing, chromatin remodeling, and DNA repair (for recent reviews, see refs *1*−*5*). The precise coordination of these events is orchestrated by different phosphorylation patterns on the CTD of RNAPII, which allow interaction with specific factors, such as splicing and capping factors (*1*−*5*).

In humans, the CTD of RNAPII is comprised of 52 repeats of the heptapeptide sequence Y-S-P-T-S-P-S (*6, 7*). The CTD becomes extensively phosphorylated during the early stage of transcription and stays highly phosphorylated during transcript elongation. Dephosphorylation of the CTD is required to recycle RNAPII, so that it can reinitiate transcription and pursue another round of transcription (*8*−*12*). FCP1 is an essential component of the RNAPII transcription machinery and is known to be associated with RNAPII (*12*−*18*). FCP1 specifically dephosphorylates phosphoserine residues, mainly Ser2, of the CTD and plays a major role in RNAPII recycling (*19, 20*). In addition, FCP1 has been shown to act as a positive elongation factor (*12, 21*) and to regulate transcription promoted by the HIV-1 Tat protein (*22*).

It has been shown that the CTD phosphatase activity of FCP1 is stimulated by general transcription factor TFIIF (*23*).

[†] This work was supported by graduate scholarships from the Fonds de la Recherche en Santé du Québec and from the Université de Montréal to A.D. and a grant from the Canadian Institutes for Health Research (HOP-83068 to J.G.O. and P.L.). P.L. holds a Canada Research Chair in Structural Biology of RNA.

[‡] The NMR chemical shifts, NMR restraints, and structural coordinates have been deposited through the RCSB Protein Data Bank and given BMRB accession number 15919, RCBS entry rcsb100776, and PDB entry 2K7L, respectively.

* To whom correspondence should be addressed: Département de Biochimie, Université de Montréal, C.P. 6128, Succursale Centre-Ville, Montréal, QC, Canada H3C 3J7. Phone: (514) 343-7326. Fax: (514) 343-2210. E-mail: pascale.legault@umontreal.ca or jg.omichinski@umontreal.ca.

[§] Université de Montréal.

[||] University of Georgia.

[1] Abbreviations: 2D, two-dimensional; 3D, three-dimensional; centFCP1, central domain of FCP1; centFCP1-PO_4, centFCP1 phosphorylated at T584; CK2, casein kinase 2; COSY, correlated spectroscopy; CTD, carboxyl-terminal domain; cterFCP1, CTD of FCP1; cterRAP74, CTD of RAP74; CT-HSQC, constant-time HSQC; FCP1, TFIIF-associated CTD phosphatase; HMQC, heteronuclear multiple-quantum coherence; HSQC, heteronuclear single-quantum coherence; ITC, isothermal titration calorimetry; NOE, nuclear Overhauser effect; NOESY, NOE spectroscopy; PDB, Protein Data Bank; RAP30, RNA polymerase II-associating protein 30; RAP74, RNA polymerase II-associating protein 74; rmsd, root-mean-square deviation; RNAPII, RNA polymerase II; TAD, transactivation domain; TOCSY, total correlation spectroscopy; TFIIF, general transcription factor IIF.

10.1021/bi801549m CCC: $40.75
Published on Web 02/12/2009

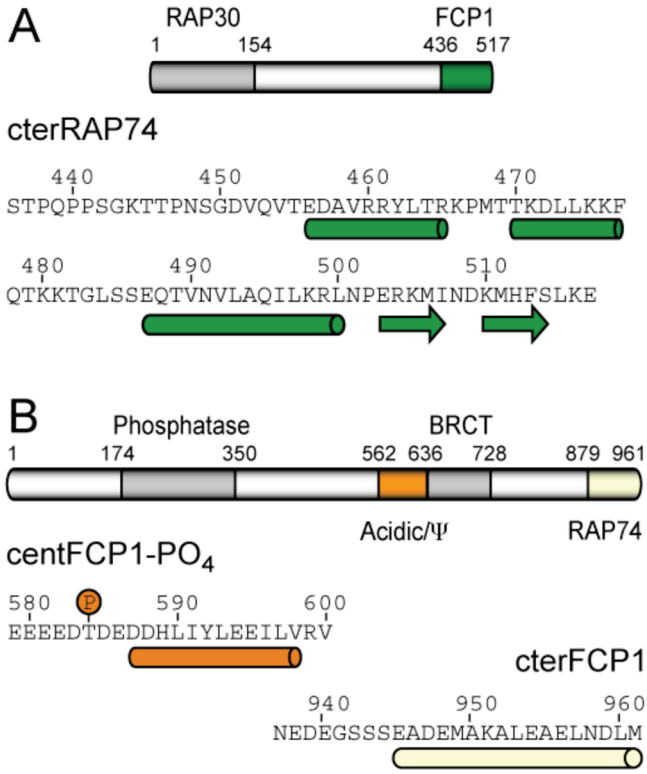

FIGURE 1: cterRAP74, centFCP1-PO_4, and cterFCP1 fragments used for this study. (A) Domain organization of human RAP74 and primary structure of cterRAP74. RAP74 contains a RAP30-binding domain (*28*) and an FCP1-binding domain (*30*). (B) Domain organization of human FCP1 and primary structures of centFCP1-PO_4 and cterFCP1. FCP1 contains a phosphatase domain (*71*), an acidic/hydrophobic (Ψ) domain (*22*), a BRCT (breast cancer protein-related carboxy-terminal) homology domain (*22*), and a C-terminal RAP74-binding domain (*30*). The elements of secondary structure derived from the NMR structure of the centFCP1-PO_4−cterRAP74 complex (this study) and the cterFCP1−cterRAP74 complex (*33*) are depicted below the sequences.

Human TFIIF is composed of large (RAP74) and small (RAP30) subunits (*24*−*26*). The RAP74 subunit also contacts TFIIB, RNAPII, and FCP1 and through these interactions helps regulate initiation, elongation, termination, and polymerase recycling (*15, 22, 27*−*32*). The main role of RAP74 in termination and polymerase recycling may be to stimulate the CTD phosphatase activity of FCP1 (*13*). Previous studies demonstrated that both the central and C-terminal domains of FCP1 interact independently and specifically with the C-terminal domain of RAP74 [cterRAP74 (Figure 1)], suggesting that these interactions are responsible, in part, for the ability of TFIIF to stimulate the CTD phosphatase activity of FCP1 (*15, 22, 23, 30, 31*). Both the central and C-terminal regions of FCP1 that interact with RAP74 contain acidic/hydrophobic LXXLL-like motifs that are conserved in eukaryotes (*22, 33*). Furthermore, both the central and C-terminal RAP74-binding sites of FCP1 are adjacent to conserved casein kinase 2 (CK2) phosphorylation sites (*34*−*36*). In vitro studies examining the role of CK2 in FCP1 function demonstrated that phosphorylation not only enhances RAP74 binding but also stimulates CTD phosphatase activity (*34, 35*). We previously demonstrated that CK2 phosphorylation of either T584 in a central FCP1 peptide or S942 and S944 in the C-terminal domain of FCP1 leads to enhanced binding to cterRAP74 (*36*). Thus, the central and C-terminal domains of FCP1 interact with RAP74 using apparently similar mechanisms, which involve their acidic/hydrophobic motif and CK2 phosphorylation of specific residues.

NMR and X-ray structural studies of free cterRAP74 and its interaction with the C-terminal domain of FCP1 have shed light on the FCP1−RAP74 interaction (*32, 33, 37, 38*). We previously determined the NMR structures of the free form of cterRAP74 [$RAP74_{436-517}$ (Figure 1A)] and of its complex with a C-terminal domain peptide of human FCP1 [cterFCP1 or $FCP1_{879-961}$ (Figure 1B)] (*32, 33*). We also performed NMR chemical shift mapping studies and found that $FCP1_{879-961}$ and $FCP1_{579-600}$ share a common binding site on RAP74 (*22*). We now present the high-resolution NMR solution structure and thermodynamic characterization by isothermal titration calorimetry (ITC) of a complex formed by cterRAP74 and a phosphorylated peptide from the central domain of FCP1 [centFCP1-PO_4 or $FCP1_{579-600}$-T584PO_4 (Figure 1B)]. We compare the NMR structure of the centFCP1-PO_4−cterRAP74 complex with our previously determined NMR structure of the cterFCP1−cterRAP74 complex (*33*) and assess the role of specific residues on the basis of our NMR and ITC data.

EXPERIMENTAL PROCEDURES

Production and Purification of cterRAP74 and FCP1 Peptides. The C-terminal domain of RAP74 (Figure 1A) was expressed from a GST-2T vector (GE Healthcare) as a GST fusion protein in *Escherichia coli* strain Topp2 cells (Stratagene) (*15*). Site-directed mutagenesis was performed using the QuickChange II site-directed mutagenesis kit (Stratagene) and verified by DNA sequencing. The cterRAP74 domain and related mutants were expressed and purified as previously described (*32*). The FCP1 peptides [centFCP1, centFCP1-PO_4, and cterFCP1 (Figure 1B)] were synthesized and purified as described previously (*22, 36*).

NMR Samples. For NMR studies of the centFCP1-PO_4−cterRAP74 complex, the samples were prepared by titration of the unlabeled FCP1 peptide into an isotopically labeled cterRAP74 sample. The final sample compositions were 1 mM cterRAP74 (^{15}N-labeled or ^{13}C- and ^{15}N-labeled) and 1 mM unlabeled centFCP1-PO_4 in 20 mM sodium phosphate (pH 6.5) and 0.25 mM EDTA. Under these conditions, ~97% cterRAP74 and ~97% centFCP1-PO_4 were in the bound form in solution. All samples were prepared initially in a 90% H_2O/10% D_2O mixture. For studies in D_2O, the samples were transferred to 99.996% D_2O with multiple cycles of lyophilization and resuspension. The 2D ^{1}H−^{15}N HSQC spectra (*39*) and the 2D ^{13}C/^{15}N-{F_1/F_2}-filtered ^{1}H−^{1}H NOESY spectra (*40*) of the centFCP1-PO_4−[^{15}N,^{13}C]cterRAP74 complex did not change during the course of NMR data collection, indicating that the complex is very stable, and that T584 remained phosphorylated during the course of NMR data collection (*36*).

NMR Spectroscopy. All NMR experiments were conducted at 300 K on a Varian ^{Unity}INOVA 600 MHz NMR spectrometer equipped with a pulse-field gradient unit and an actively shielded z-gradient HCN triple-resonance probe (either a room-temperature probe or a cryogenic probe). The backbone and aliphatic side chain resonances (^{1}H, ^{15}N, and ^{13}C) of cterRAP74 were assigned using a combination of NMR experiments, including 2D ^{1}H−^{15}N HSQC (*39*), 2D

$^1H-^{13}C$ constant time (CT) HSQC (*41, 42*), 3D HNHA (*43, 44*), 3D HNCACB (*45*−*47*), 3D HNCO (*48*), 3D (HB)CBCA-(CO)NNH (*46, 47*), 3D H(CCO)NNH-TOCSY (*47, 49*), 3D C(CO)NNH-TOCSY (*47, 49*), 3D CT HCCH-COSY (*50*), and 3D HCCH-TOCSY (*51*). The aromatic ^1H and ^{13}C signals of cterRAP74 were assigned using 2D (Hβ)Cβ(CγCδ)Hδ and (Hβ)Cβ(CγCδCε)Hε experiments (*52*). ^1H resonance assignment for centFCP1-PO_4 was achieved using 2D $^{13}C/^{15}N$-{F_1/F_2}-filtered $^1H-^1H$ TOCSY (with a DIPSI τ_m of 37.5 ms) and 2D $^{13}C/^{15}N$-{F_1/F_2}-filtered $^1H-^1H$ NOESY experiments (*40*). Intramolecular nuclear Overhauser effects (NOEs) for cterRAP74 were obtained from 3D ^{15}N-edited NOESY-HSQC (τ_m = 140 ms) (*53*) and 3D ^{13}C-edited HMQC-NOESY (τ_m = 60 and 120 ms) experiments (*54, 55*). Intramolecular NOEs for centFCP1-PO_4 were obtained from 2D $^{13}C/^{15}N$-{F_1/F_2}-filtered $^1H-^1H$ NOESY (τ_m = 40 and 100 ms) spectra (*40*) collected on a complex formed with 1 mM ^{13}C- and ^{15}N-labeled cterRAP74 and 1 mM centFCP1-PO_4. Intermolecular NOEs were obtained from 3D ^{13}C-edited HMQC-NOESY spectra (τ_m = 60 and 120 ms) (*54, 55*) and a 3D $^{13}C/^{15}N$-{F_1}-filtered-{F_3}-edited NOESY-HSQC spectrum (τ_m = 120 ms) (*56*). ^1H, ^{13}C, and ^{15}N chemical shifts were referenced to the external standard 2,2-dimethyl-2-silapentane-5-sulfonic acid (DSS) at 0.00 ppm. NMR data were processed with NMRPipe/NMRDraw (*57*) and analyzed with NMRView (*58*).

Structure Calculation. The distance restraints were subdivided into four distance ranges, strong (1.8−2.8 Å), medium (1.8−3.4 Å), weak (1.8−5.0 Å), and very weak (1.8−6.0 Å), by comparison with NOEs involving protons separated by known distances within the α-helical elements (residues 456−465, 470−477, and 487−500 of cterRAP74). An extra 0.5 or 1.0 Å was added to the upper distance limit for restraints involving methyl protons (0.5 Å), methylene protons (0.5 Å), and the H^δ/H^ε protons of Phe and Tyr residues (1.0 Å). A total of 1640 NOE-derived distance restraints were obtained for structure calculation (Table 1). Residues 436−450 at the amino terminus of cterRAP74 and residues 579−581 at the amino terminus of centFCP1-PO_4 did not display any medium-range, long-range, or intermolecular NOE, and these residues were therefore not included in the structure calculation. Backbone dihedral angle restraints (ϕ and ψ angles) were obtained from analysis of H^α, H^N, C^α, C^β, C', and N^H chemical shifts using TALOS (*59*). The error values on dihedral angle restraints (±10° to ± 45°) were either twice that obtained from the TALOS analysis or given a minimum value of 10°. A total of 135 TALOS-derived dihedral angle restraints (ϕ and ψ angles) were used for structure calculation. Structures were calculated using the torsion angle molecular dynamics protocol of CNS (*60*) starting from two extended structures (one of cterRAP74 and one of centFCP1-PO_4) with standard geometry. CNS topology and parameter files for the phosphorylated threonine residues were obtained from HIC-Up (*61*). In addition to standard protein covalent geometry and NMR-derived restraints (Table 1), the force field included a van der Waals repulsive term and a conformational database potential (*62*), but neither hydrogen bonding nor electrostatic terms were used at any stage of the structure calculation. An ensemble of 20 structures that satisfied the experimental restraints (no distance violation of >0.2 Å and no torsion angle violation of >5°) was calculated. These 20 structures were used to compute an average structure that was minimized against experimental restraints. Structural statistics (Table 1) were obtained from CNS and PROCHECK-NMR (*63*). All figures were generated using PyMOL (*64*).

Table 1: Structural Statistics of the centFCP1-PO_4−cterRAP74 Complex[a]

restraints used for structure calculation	
total no. of NOE distance restraints	1640
intraresidue	788
interresidue sequential (i, i + 1)	339
interresidue medium-range (1 < $\|i - j\|$ < 5)	254
long-range ($\|i - j\| \geq 5$)	200
intermolecular	59
no. of dihedral angle restraints (ϕ and ψ)	135
structural statistics	
rmsd from idealized geometry	
bonds (Å)	0.0034 ± 0.0001
angles (deg)	0.49 ± 0.01
impropers (deg)	0.31 ± 0.01
rmsd from distance restraints (Å)	0.0242 ± 0.0007
rmsd from dihedral angle restraints (deg)	0.32 ± 0.05
Ramachandran analysis (%)	
most favored regions	80.7
additionally allowed regions	17.8
generously allowed regions	1.4
disallowed regions	0.1
atomic pairwise rmsd (Å)	
centFCP1-PO_4−cterRAP74 complex	
backbone atoms (C', C^α, N) for secondary structure[b]	0.30 ± 0.07
backbone atoms (C', C^α, N)	0.74 ± 0.24
all heavy atoms	1.05 ± 0.20
cterRAP74 alone	
backbone atoms (C', C^α, N) for secondary structure[b]	0.29 ± 0.06
backbone atoms (C', C^α, N)	0.59 ± 0.22
all heavy atoms	0.93 ± 0.22
centFCP1-PO_4 alone	
backbone atoms (C', C^α, N) for secondary structure[b]	0.22 ± 0.09
backbone atoms (C', C^α, N)	0.88 ± 0.43
all heavy atoms	1.20 ± 0.35

[a] Only residues 451−517 of cterRAP74 and residues 582−600 of centFCP1-PO_4 were included in the structure calculation. [b] The secondary structure for cterRAP74 is composed of helix H1 (E456−R465), helix H2 (T470−F477), helix H3 (E487−L500), strand S1 (E503−I507), and strand S2 (K510−S514). The secondary structure for centFCP1-PO_4 is the H1′ helix (D587−V598).

ITC Studies. The FCP1 peptides and cterRAP74 prepared for ITC studies were extensively dialyzed against 20 mM sodium phosphate (pH 6.2) and 0.25 mM EDTA. The concentrations of the cterRAP74, centFCP1, and centFCP1-PO_4 peptides were derived from the absorbance at 280 nm using an extinction coefficient of 1490 cm^{-1} M^{-1} (*65*). The concentration of the cterFCP1 peptide was calculated on the basis of weight measurements. All peptides were degassed at 295 K for 5 min before each experiment. ITC measurements were performed at 300 K using a VP-ITC microcalorimeter (MicroCal, Northhampton, MA). The concentration of cterRAP74 in the cell was between 15 and 50 μM, and the concentration of FCP1 peptide in the syringe was 10 times higher than that of cterRAP74. Under these conditions, the c value ([cterRAP74]/K_D) was between 1 and 200, a range that allows accurate thermodynamic parameters to be extracted (*66*).

Data collected for each experiment were fit to a single-binding site model. The values for the stoichiometry of binding (n) and equilibrium association constants (K_A) were determined by least-squares analysis using standard Marquardt methods and equations provided with ORIGIN version 7.0. The quality of the fit was obtained from the square of the correlation coefficient (R^2), and in all cases, $R^2 \geq 0.99$. The dissociation constant K_D was calculated by taking the

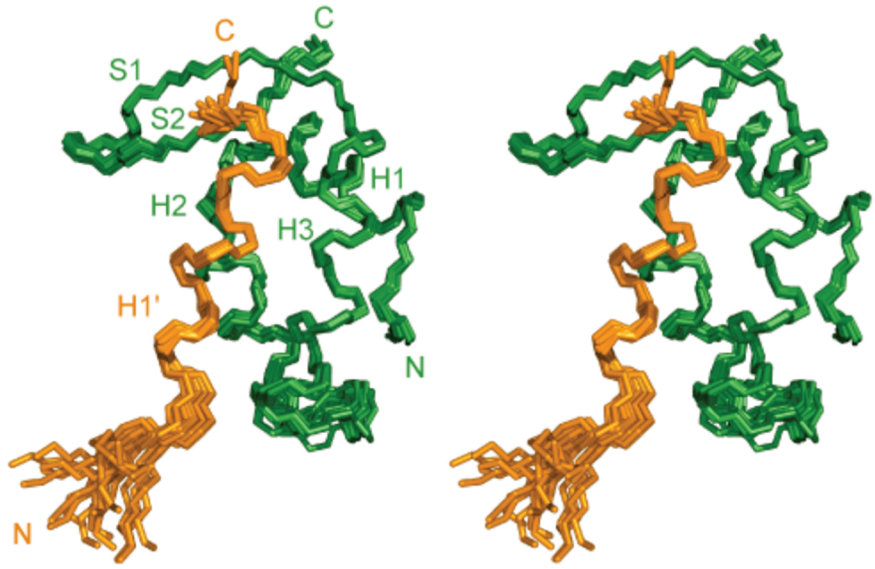

FIGURE 2: Superposition of the 20 NMR structures of the centFCP1-PO_4−cterRAP74 complex. Each structure is shown as a stereoview of the backbone trace (N, C^{α}, and C′) for residues 453−517 of RAP74 (green) and for residues 582−600 of FCP1 (orange).

inverse of K_A. The free energy (ΔG) was calculated from the relationship $\Delta G = RT \ln K_D$, where R denotes the gas constant and T is the temperature (300 K). Multiple ITC experiments (at least three) were conducted for each complex, and the reported values and errors on the thermodynamic parameters (n, K_D, and ΔG) are the average and standard deviations from these measurements, respectively.

RESULTS

Structure of cterRAP74 in the Complex. In the complex with centFCP1-PO_4 (Figure 2), cterRAP74 adopts a winged-helix fold, an $\alpha\beta$ topology consisting of three consecutive α-helices (H1, E456−R465; H2, T470−F477; and H3, E487−L500), followed by an antiparallel β-sheet (S1, E503−I507; and S2, K510−S514). These five elements of secondary structures are assembled via four interconnecting loops (L1, L2, L3, and L4), with L2 being the region of the protein that is the least well defined by the NMR data (Figure 2). Superpositions of cterRAP74 from the minimized average structure of the complex determined here with its free form (*32*) and its cterFCP1-bound form (*33*) yielded backbone rmsd values for residues 451−517 of 1.52 and 1.69 Å, respectively (not shown). Although overall these structures of cterRAP74 are similar, it appears that there are local differences in the structure presented here when compared to the two previously determined NMR structures.

Structure of centFCP1-PO_4 in the Complex. In the complex, centFCP1-PO_4 adopts a 12-residue amphipatic α-helix (H1′) between residues D587 and V598. The orientation of the H1′ helix is well-defined with respect to cterRAP74, in agreement with the large number of intermolecular NOEs involving residues from this helix (Table S1 and Figure S1 of the Supporting Information). By contrast, the N-terminal acidic region of the peptide containing T584PO_4 is not well defined (Figure 2), which is consistent with the paucity of NOEs for this region.

Interface of the centFCP1-PO_4−cterRAP74 Complex. Helices H2 and H3 of cterRAP74 constitute the primary interacting surface, forming a hydrophobic groove that is large enough to accommodate the three turns of the H1′ α-helix from centFCP1-PO_4 (Figure 3A). The nonpolar face of helix H1′ docks in the hydrophobic groove of cterRAP74 (Figure 3A). Four residues of centFCP1-PO_4 (L590, L593, L597, and V598) are inserted in this groove and act as hydrophobic anchors. We distinguish the C-terminal (L597 and V598) from the central hydrophobic anchors (L590 and L593), according to their relative locations in the H1′ helix (Figure 3A). The side chains of L597 and V598 from FCP1 project deeply into a hydrophobic pocket on the cterRAP74 surface, and they are almost completely buried (Figure 3A and Figure S2 of the Supporting Information). The two side chains of the central hydrophobic anchors, L590 and L593, interact with smaller adjacent hydrophobic pockets on the surface of cterRAP74 (Figure 3A and Figure S2 of the Supporting Information).

The interaction between the highly basic cterRAP74 and the highly acidic centFCP1-PO_4 also involves electrostatic forces. Basic residues K471, K475, K480, K481, K498, and R499 of cterRAP74 surround the hydrophobic groove defined by helices H2 and H3 (Figure 3B). There are two acidic regions in centFCP1-PO_4, an extensive one at the N-terminus containing 11 acidic residues (E579−D588) and a short one formed by residues E594 and E595 (Figures 1B and 3B). It appears that most of the acidic residues in centFCP1-PO_4 and the basic residues lining the hydrophobic groove of cterRAP74 participate in long-range nonspecific intermolecular electrostatic interactions (Figure 3B). We identified only two specific ionic interactions (salt bridges) between cterRAP74 and centFCP1-PO_4. One is formed between E594 of centFCP1-PO_4 and K471 of cterRAP74 (Figure 3B). In the energy-minimized average structure, the shortest distance between the O^{ε} atoms of E594 and the H^{ε} atoms of K471 is 3.3 Å. Many intermolecular NOEs help position the side chains of E594 (FCP1) and K471 (RAP74) in the structure (Table S1 and Figure S1 of the Supporting Information); thus, the E594−K471 salt bridge is well-defined by the NMR data. Interestingly, E594 is also positioned to form an intramolecular salt bridge with R599 that may stabilize the C-terminus of the H1′ helix (Figure 3B). The other intermolecular salt bridge is formed between D587 of centFCP1-

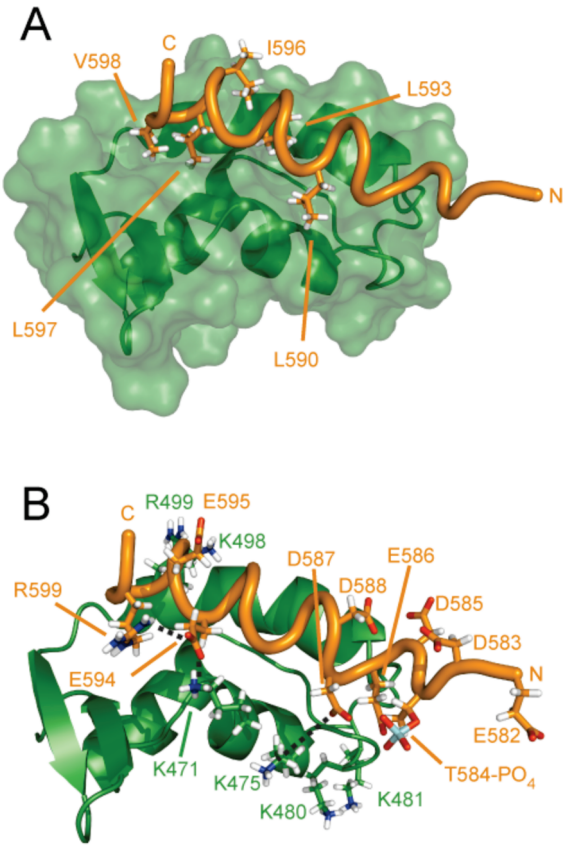

FIGURE 3: Summary of the intermolecular interactions in the centFCP1-PO_4−cterRAP74 complex. (A) van der Waals interactions at the interface of the complex. The three-dimensional structure of cterRAP74 is shown as a ribbon within the transparent molecular surface (green, residues 451−517), whereas centFCP1-PO_4 is represented as a backbone trace (orange, residues 582−600). The side chains of all the hydrophobic residues from centFCP1-PO_4 that participate in van der Waals contacts with cterRAP74 are shown as sticks. (B) Electrostatic interactions at the interface of the complex. The side chains of all the charged residues from centFCP1-PO_4 and of the basic residues from cterRAP74 lining the hydrophobic groove are shown as sticks. Intermolecular salt bridges are found between K471 of RAP74 and E594 of FCP1 and between K475 of RAP74 and D587 of FCP1.

PO_4 and K475 of cterRAP74 (Figure 3B). Given the low density of intermolecular NOEs involving residues at the N-terminus of centFCP1-PO_4 (Table S1 and Figure S1 of the Supporting Information), the D587−K475 salt bridge is less well defined by the NMR data. Residue K475 is also near two other acidic side chains: E586 and T584PO_4 of centFCP1-PO_4 (Figure 3B). The shortest distances between the H^{ϵ} atom of K475 and the side chain oxygen atoms of D587, E586, and T584PO_4 in the average structure are 6.5, 9.3, and 9.6 Å, respectively. These distances indicate that the D587−K475 salt bridge is not as strong as the E594−K471 salt bridge and that the side chains of E586 and T584PO_4 do not participate in strong intermolecular ionic interactions.

Role of T584 Phosphorylation. We performed ITC studies to assess the effect of T584 phosphorylation on cterRAP74 binding (Figure 4 and Table 2). We obtained a K_D of 2.1 ± 0.9 μM for the binding of centFCP1 to cterRAP74 and a K_D of 0.7 ± 0.1 μM for the binding of centFCP1-PO_4 to cterRAP74 (Table 2). This 3-fold decrease in K_D translates to a reduction of 0.7 kcal/mol in free energy, indicating that T584PO_4 makes only a minor contribution to the interaction

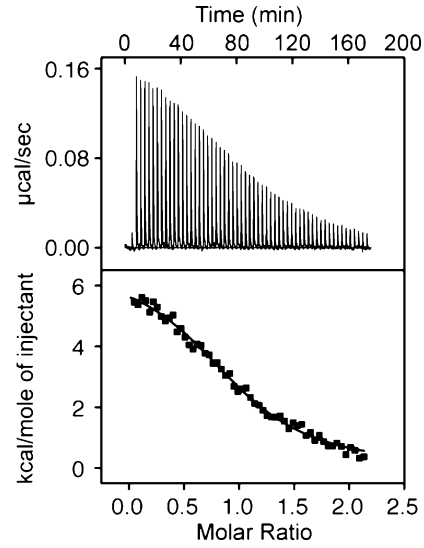

FIGURE 4: Representative ITC data of cterRAP74 binding to centFCP1 at 300 K in a buffer containing 20 mM sodium phosphate (pH 6.2) and 0.25 mM EDTA. From this ITC experiment, we obtained a K_D of 2.88 μM and a stoichiometry (n) of 1.02.

Table 2: Thermodynamic Parameters for the Association of FCP1 Peptides with cterRAP74

FCP1 peptide	cterRAP74	n	K_D (μM)	ΔG (kcal/mol)
centFCP1	wild type	0.8 ± 0.1	2.1 ± 0.9	−7.8 ± 0.3
centFCP1	K471E	ND[a]	ND[a]	ND[a]
centFCP1	K475E	0.9 ± 0.1	34 ± 2	−6.13 ± 0.04
centFCP1-PO_4	wild type	0.9 ± 0.1	0.7 ± 0.1	−8.45 ± 0.09
centFCP1-PO_4	K471E	ND[a]	ND[a]	ND[a]
centFCP1-PO_4	K475E	1.0 ± 0.2	18 ± 2	−6.51 ± 0.07
cterFCP1	wild-type	1.01 ± 0.02	0.5 ± 0.1	−8.7 ± 0.2

[a] No detectable binding.

of centFCP1-PO_4 with cterRAP74. In the NMR structure of the complex, T584PO_4 is located too far from the interface to participate in any energetically significant dipolar, hydrogen bonding, or ionic interactions (Figure 3B). However, T584PO_4 likely contributes to a network of weak long-range intermolecular ionic interactions involving the negatively charged N-terminal domain of the FCP1 peptide and a positively charged patch on the surface of cterRAP74 composed of four lysine residues (Figure 3B). The small change in the free energy of binding provided by phosphorylation of T584 is therefore in agreement with the lack of significant interactions involving T584PO_4 in the structure of the centFCP1-PO_4−cterRAP74 complex.

Role of Ionic Interactions in cterRAP74. To evaluate the importance of individual ionic interactions in the complex, we prepared point mutants of cterRAP74 in which specific lysine residues were converted to glutamate (K471E and K475E mutants) and investigated their binding to centFCP1 and centFCP1-PO_4 by ITC (Table 2). The K471 residue of cterRAP74 forms a strong ionic interaction with E594 in the structure of the centFCP1-PO_4−cterRAP74 complex (Figure 3B). We therefore expected that the K471E mutation would cause a dramatic decrease in affinity for both the centFCP1 and centFCP1-PO_4 peptides, and this is what we observed. The binding of both FCP1 peptides to cterRAP74-K471E was undetectable ($K_D \geq 150$ μM). Thus, both the NMR and ITC data provide evidence that K471 plays a crucial role in the interaction of centFCP1 with RAP74. Similarly, K475 of cterRAP74 forms a salt bridge with D587 of centFCP1-

PO_4 (Figure 3B), and the K_D values for binding of the K475E mutant to centFCP1 and centFCP1-PO_4 are ~15−25-fold higher than that of wild-type cterRAP74 (Table 2). Therefore, these results confirm that K475 makes a significant contribution to the interaction with centFCP1. In addition, the ITC data with the cterRAP74 mutants are in agreement with the lack of significant ionic interactions involving T584PO_4.

Comparison of ITC and NMR Data for the centFCP1-PO_4−cterRAP74 and cterFCP1−cterRAP74 Complexes. The ITC data reveal that centFCP1-PO_4 and cterFCP1 bind to cterRAP74 with similar affinities. For the cterFCP1−cterRAP74 complex, we measured a K_D of 0.5 ± 0.1 μM, which is essentially identical to the K_D of 0.7 ± 0.1 μM measured for the centFCP1-PO_4−cterRAP74 complex (Table 2).

To compare the interactions of centFCP1-PO_4 and cterFCP1 with cterRAP74, we first computed the differences in H^N, C′, and N^H chemical shifts for cterRAP74 between its two bound forms. This analysis revealed that 26 of the 70 amino acid residues analyzed (residues 448−517 of cterRAP74) displayed significant chemical shift differences ($\Delta\delta$ > 0.15 ppm; see Figure 5A). When mapped onto the NMR structure of the centFCP1-PO_4−cterRAP74 complex, the residues displaying significant differences in chemical shift are predominantly located in the H2 and H3 helices and adjoining loop L2 (Figure 5B). The H2 and H3 helices form the binding groove for the two FCP1 peptides; therefore, changes in chemical shifts in these helices could be due to a different binding interface, structural differences in cterRAP74 between the two complexes, or both. Residues from adjoining loop L2, however, do not interact with either peptide. The chemical shift mapping therefore suggests that the L2 loop adopts a different structure in the two complexes, and this was indeed confirmed by the NOE data. Specifically, we observed four long-range NOEs between V452 of the N-terminal segment of cterRAP74 and F477, K481, and T482 of the L2 loop, but these NOEs were not observed in the cterFCP1−cterRAP74 complex (*33*). The role of the L2 loop may be to fine-tune the structure of the binding groove formed by helices H2 and H3 to create a surface that is complementary to a specific FCP1 sequence.

Structural Comparison of the centFCP1-PO_4−cterRAP74 and cterFCP1−cterRAP74 Complexes. To provide a detailed understanding of how cterRAP74 interacts with the two related but different FCP1 peptides, we superposed the NMR structures of the centFCP1-PO_4−cterRAP74 and cterFCP1−cterRAP74 complexes (Figure 6). This superposition was based on rmsd minimization for backbone atoms of cterRAP74 within the well-defined secondary structure elements (rmsd = 1.15 Å). The overall structure of cterRAP74 in these two complexes is very similar, although the orientation of individual secondary structural elements and connecting loops varies with respect to one another (Figure 6A). Both FCP1 peptides interact with cterRAP74 via an α-helical segment: the centFCP1-PO_4 peptide adopts a 12-residue α-helix (residues 587−598), whereas the cterFCP1 peptide adopts a longer 17-residue α-helix (residues 945−961) (*33*). There is a more extensive binding interface for cterFCP1 compared to centFCP1; the total solvent-accessible surface area buried by complex formation is 1160 Å^2 for the centFCP1-PO_4−cterRAP74 complex, whereas it is 1510 Å^2 for the cterFCP1−cterRAP74 complex (*33*). Another important difference between the two complexes is that the

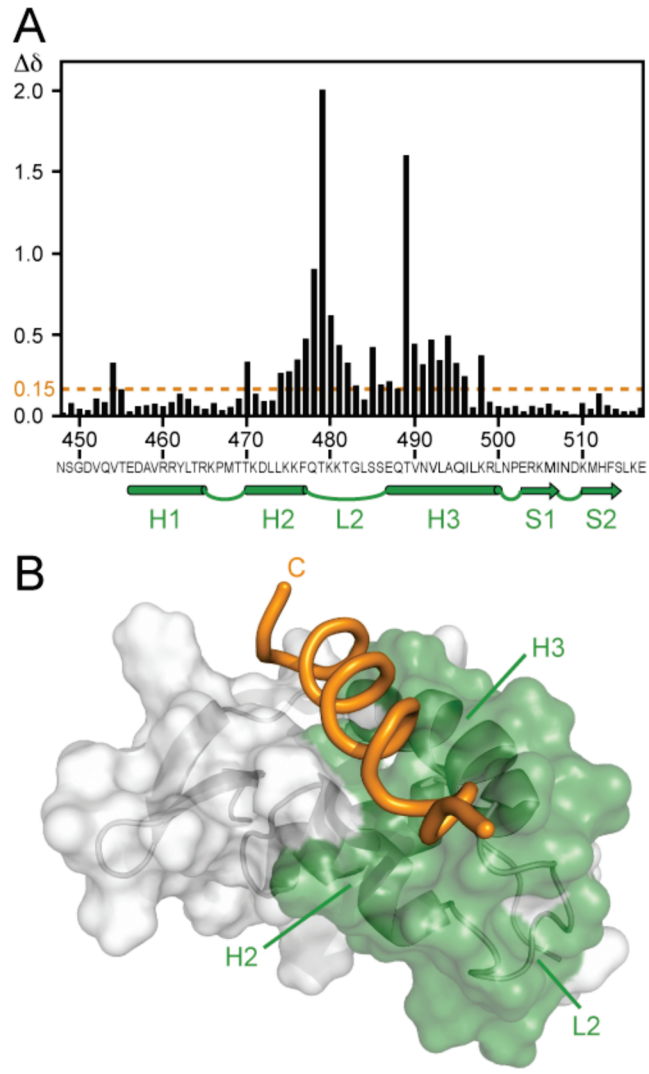

FIGURE 5: (A) Histogram of the differences in chemical shifts between the centFCP1-PO_4−cterRAP74 and cterFCP1−cterRAP74 complexes (*33*). The differences were calculated with the formula $\Delta\delta = [(\Delta H^N)^2 + (0.17\Delta N^H)^2 + (0.39\Delta C')^2]^{1/2}$ and are given in parts per million. (B) Residues that show significant chemical shift differences ($\Delta\delta$ > 0.15 ppm) are colored green on the NMR structure of the centFCP1-PO_4−cterRAP74 complex.

cterFCP1 peptide inserts more deeply in the groove formed by helices H2 and H3, especially near the L2 loop. When bound to the cterFCP1 peptide, cterRAP74 adopts a more open conformation, where the N-terminus of helix H3 is shifted ~4.0 Å from the C-terminus of helix H2 (Figure 6A, right). This structural difference is supported by NOE data, since we observed six long-range NOEs between Q478 at the C-terminus of helix H2 and residues S486, E487, and T489 at the N-terminus of helix H3 in the centFCP1-PO_4−cterRAP74 complex, whereas these NOEs were not observed in either the free form or the cterFCP1-bound form of cterRAP74. There are clearly some local differences within the FCP1-binding site of cterRAP74 between the two complexes, indicating that cterRAP74 adjusts its conformation to optimize its interaction with the centFCP1-PO_4 peptide.

Both the centFCP1-PO_4 and cterFCP1 peptides make significant van der Waals contacts with hydrophobic residues of cterRAP74. For the centFCP1-PO_4 peptide, we identified both central (L593 and L590) and C-terminal (V598 and

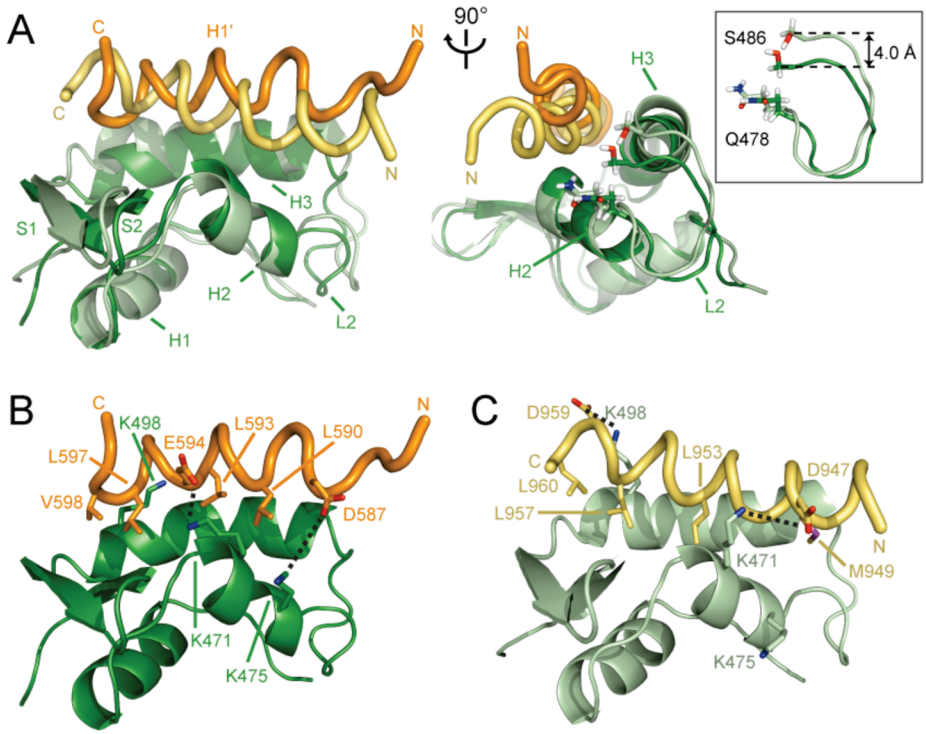

FIGURE 6: Structural comparison of two FCP1−RAP74 complexes: the centFCP1-PO_4−cterRAP74 and cterFCP1−cterRAP74 complexes (PDB entry 1ONV) (*33*). (A) Superposition of the two complexes based on rmsd minimization for backbone atoms of cterRAP74 within the well-defined secondary structure elements. The centFCP1-PO_4−cterRAP74 complex is shown in dark colors (green for RAP74 and orange for FCP1), and the cterFCP1−cterRAP74 complex is shown in light colors (pale green for RAP74 and pale yellow for FCP1). A close-up of the loop between H2 and H3 is shown with the side chains of Q478 and S486 to emphasize a significant difference in the RAP74 structure between the two complexes. (B and C) Comparisons of intermolecular interactions between the two complexes. Only relevant side chains are shown. In panel B, the shortest $H^{\varepsilon}-O^{\varepsilon}/O^{\delta}$ distances for the K471−E594 and K475−D587 salt bridges are 3.3 and 6.5 Å, respectively. In panel C, the shortest $H^{\varepsilon}-O^{\delta}$ distances for the K498−D959 and K471−D947 salt bridges are 2.2 and 4.2 Å, respectively. For clarity, the complexes in panels B and C are shown in the same orientation and colors as in the left portion of panel A.

L597) hydrophobic anchors (Figure 6B). For the cterFCP1 peptide, there are also one central (L953) and two C-terminal (L960 and L957) hydrophobic anchors, but in addition, there is an important N-terminal hydrophobic anchor [M949 (Figure 6C)]. The interactions with the side chain of M949 allow the N-terminus of cterFCP1 to be buried more deeply than centFCP1-PO_4 (~3.0 Å) in the hydrophobic groove of cterRAP74.

There are two salt bridges in each of the two FCP1−RAP74 complexes, and K471 appears to play a central role in both complexes. In the centFCP1-PO_4−cterRAP74 complex, the N^{ε} atom of K471 extends toward the C-terminus of centFCP1-PO_4, forming a strong salt bridge with E594 (Figure 6B). In contrast, the N^{ε} atom of K471 extends toward the N-terminus of cterFCP1 and forms a salt bridge with D947 (Figure 6C). In the centFCP1-PO_4−cterRAP74 complex, K475 of cterRAP74 forms a second salt bridge with D587 at the N-terminus of centFCP1-PO_4 (Figure 6B). In the cterFCP1−cterRAP74 complex, the second salt bridge involves D959 at the C-terminus of cterFCP1 and K498 of cterRAP74 (Figure 6C). Thus, the pattern of intermolecular ionic interactions in the two FCP1−RAP74 complexes is very different.

Structure-Based Sequence Comparison between centFCP1 and cterFCP1. We have previously aligned the LXXLL-like motifs present within the RAP74-binding domains of centFCP1 and cterFCP1 (*36*). In this alignment, the L593−L597 segment of centFCP1 corresponded to the L957−M961 segment of cterFCP1. However, it is now clear that residues L593 and L597 of centFCP1-PO_4 make very similar contacts with cterRAP74 as residues L953 and L957 of cterFCP1 (Figure 6). We used this structural similarity as a basis for the sequence alignment shown in Figure 7A. Other hydrophobic residues of FCP1 that participate in important van der Waals contacts are nearby in the sequence alignment as well as in the three-dimensional structures: L590 of centFCP1, which corresponds to M949 in cterFCP1, and V598 of centFCP1, which corresponds to L960 in cterFCP1. It is interesting to note that within this structure-based alignment, two residues that are phosphorylated by CK2, T584 of centFCP1 and S942 of cterFCP1, are found at equivalent positions. Two residues that make a salt bridge interaction with cterRAP74, D587 of centFCP1 and D947 of cterFCP1, are also found at equivalent positions. Surprisingly, these residues contact different lysine residues in cterRAP74 (Figure 6). For the two other important residues that form salt bridges (E594 of centFCP1 and D959 of cterFCP1), there is no such sequence or structural resemblance. However, E954 in cterFCP1, which corresponds to E594 of centFCP1 in our new alignment (Figure 7A), contributes to RAP74 binding through polar interaction with T470 (*33*). An interesting outcome of this structure-based alignment is the realization that residues from centFCP1 and cterFCP1 that are at equivalent positions in the sequence alignment (e.g., D587 and D947; E594 and E954) participate in intermolecular interactions with different residues of RAP74.

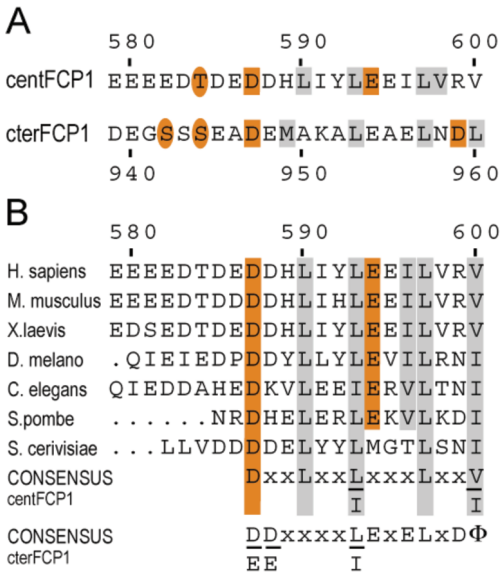

FIGURE 7: Structure-based sequence alignments of centFCP1 from *Homo sapiens* (NP_004706.2) with (A) cterFCP1 from *H. sapiens* and (B) centFCP1 from various eukaryotes: *Mus musculus* (AAH53435), *Xenopus laevis* (AAK27686), *Drosophila melanogaster* (Q9W147), *Caenorhabditis elegans* (NP_492423), *Schizosaccharomyces pombe* (Q9P376), and *Saccharomyces cerevisiae* (NP_014004). The numbers in parentheses are GenBank accession numbers, except for that of *D. melanogaster*, which is from the Swiss-Prot Database. In panel A, the hydrophobic residues (gray) and ionic residues (orange) that participate in important interactions with cterRAP74 are boxed and the residues phosphorylated by CK2 are circled. In panel B, residues conserved in all or almost all species are highlighted using the following color code: orange for acidic residues (D and E) and gray for hydrophobic residues (I, L, M, and V). A consensus sequence is provided for centFCP1 based on this alignment, and the previously derived consensus for cterFCP1 is shown for the sake of comparison (*33*).

On the basis of the structural information, we also aligned sequence segments of centFCP1 from several other eukaryotic FCP1 proteins (Figure 7B). Of the four hydrophobic residues of centFCP1 that act as hydrophobic anchors in the complex with cterRAP74, three (L590, L593, and L597) are conserved in this alignment. The fourth hydrophobic residue, V598, is only found in the *H. sapiens*, *M. musculus*, and *X. laevis* sequences. Given that V600 is conserved as a valine or an isoleucine in all FCP1 sequences, we propose that, in certain species, V600 (or I600) may substitute for V598, similarly to L960 of cterFCP1 (Figures 6B,C and 7A). We also found that the two residues in centFCP1 that participate in salt bridges with cterRAP74, D587 and E594, are strictly and highly conserved, respectively. In summary, there is an excellent correlation between the conserved residues within the RAP74-binding domain of centFCP1 and the residues that play an important role in defining the centFCP1−cterRAP74 interface, pointing to the importance of this interaction through evolution.

DISCUSSION

With this work, we clearly demonstrated that like cterFCP1, centFCP1-PO_4 interacts with the basic/hydrophobic groove formed by helices H2 and H3 on the surface of cterRAP74. Our studies reveal the importance of two leucine residues in each RAP74-binding domain of human FCP1 (L593 and L597 in centFCP1 and L953 and L957 in cterFCP1) that are found at equivalent positions in the alignment and make similar interactions with cterRAP74. In agreement with these observations, mutation of leucine residues in either the central (L593A) or C-terminal domain (L957A) was found to significantly reduce the level of binding to cterRAP74 in vitro (*22, 33*). However, it appears that the RAP74-binding domains of centFCP1 and cterFCP1 have little in common besides these two conserved leucine residues. Indeed, the consensus RAP74-binding sequence of centFCP1 is fairly different from the reported consensus sequence for cterFCP1 (Figure 7B) (*33*). Clearly, the terminology "LXXLL-like motif" previously used to describe the RAP74-binding domains of centFCP1 and cterFCP1 is no longer adequate and should be replaced by "L/IxxxL motif".

A detailed structural comparison revealed significant differences between the centFCP1-PO_4−cterRAP74 and cterFCP1−cterRAP74 complexes, even though their dissociation constants are essentially identical. This structural comparison points out the remarkable adaptability of the cterRAP74 binding groove to provide shape and charge complementary to the different FCP1 peptides. This type of adaptability may be common in protein−protein interactions. For example, we previously determined two NMR structures involving the Tfb1 (yeast)/p62 (human) subunit of the general transcription factor TFIIH and an acidic transactivation domain (TAD): the p53 TAD−Tfb1 complex (*67*) and the VP16 TAD−Tfb1 complex (*68*). In these complexes, we found that both the p53 and VP16 TADs interact with the same binding surface on the PH domain of Tfb1. Although there were several similarities between the two structures, there were also important differences despite the fact that both TADs bind Tfb1 with comparable affinities (*67, 68*).

Our ITC studies demonstrate that cterRAP74 interacts with similar affinity with both the central and C-terminal domains of FCP1. The functional implication(s) of this phenomenon is not yet understood. It has been shown that two RAP74−RAP30 heterodimers associate via homomeric RAP74 interactions to form an $\alpha_2\beta_2$ heterotetramer (*18, 69*). Given the similar affinity of the two FCP1 domains for cterRAP74, these two domains of FCP1 may bind simultaneously to the two RAP74 subunits of the TFIIF heterotetramer in vivo. Alternatively, assembly of the TFIIF heterotetramer and its interaction with RNAPII may cause conformational changes in TFIIF that affect differently the affinity of the two interacting domains of FCP1 for cterRAP74. In this scenario, differential states of TFIIF (and/or RNAPII) would affect the formation of the TFIIF−FCP1 complex, which, in turn, may modulate the different roles of FCP1 in transcription regulation.

The fact that both the central and C-terminal domains of FCP1 interact with cterRAP74 could also be an example of biological redundancy that insures the recruitment of FCP1 to the RNAPII complex and the activation of its phosphatase activity. C-Terminal deletion mutants of FCP1, in which the two RAP74-binding domains are absent, are not viable in yeast (*16*) and are severely affected in humans (*70*). Indeed, individuals affected with the recessive congenital cataracts facial dysmorphism neuropathy syndrome (CCFDN), associated with a truncated form of FCP1 that retains only the first 287 residues, suffer from severe development defects that affect multiple organs and systems (*70*).

The study presented here allowed us to investigate the role of T584 phosphorylation by CK2. From ITC studies, we found that T584 phosphorylation increases the affinity between centFCP1 and cterRAP74 by ~3-fold. This result is in agreement with our GST pull-down data (*36*) and is supported by the lack of significant contact involving $T584PO_4$ in the structure of the centFCP1-PO_4−cterRAP74 complex. We have previously shown that CK2 phosphorylation of T584 does not affect the interaction of centFCP1 with the HIV-1 Tat protein (*22*). CK2 phosphorylation of T584 may therefore be needed to regulate other activities of FCP1 such as its interaction with TFIIB, which also involves the central domain of FCP1 (*31, 32*). Although the role of CK2 phosphorylation in centFCP1 is not yet understood, CK2 also phosphorylates S942 and S944 of cterFCP1, and these phosphorylations likely play a significant role in strengthening the interaction between cterFCP1 and cterRAP74 (*36*). Structural and thermodynamic studies of a complex formed between cterRAP74 and a phosphorylated cterFCP1 peptide are needed to precisely define the effect of cterFCP1 phosphorylation on RAP74 binding.

ACKNOWLEDGMENT

We thank all members of the Legault and Omichinski laboratories, especially R. Richter for computer system management. We also thank E. Appella for providing the centFCP1-PO_4 peptide, L. E. Kay for providing NMR pulse sequences, and J. Archambault for critical reading of the manuscript. The 500 and 600 MHz NMR spectrometers were purchased with funds from the Canadian Foundation for Innovation, and the ITC instrument was purchased with funds from the National Sciences and Engineering Research Council of Canada.

SUPPORTING INFORMATION AVAILABLE

A list of the intermolecular NOEs used in structure calculation (Table S1), intermolecular NOE data from the 3D $^{13}C/^{15}N$-{F_1}-filtered-{F_3}-edited NOESY-HSQC spectrum (Figure S1), and close-up views of the hydrophobic interactions between centFCP1 and cterRAP74 (Figure S2). This material is available free of charge via the Internet at http://pubs.acs.org.

REFERENCES

1. Meinhart, A., Kamenski, T., Hoeppner, S., Baumli, S., and Cramer, P. (2005) A structural perspective of CTD function. *Genes Dev. 19*, 1401–1415.
2. Phatnani, H. P., and Greenleaf, A. L. (2006) Phosphorylation and functions of the RNA polymerase II CTD. *Genes Dev. 20*, 2922–2936.
3. Hirose, Y., and Ohkuma, Y. (2007) Phosphorylation of the C-terminal domain of RNA polymerase II plays central roles in the integrated events of eucaryotic gene expression. *J. Biochem. 141*, 601–608.
4. Cho, E. J. (2007) RNA polymerase II carboxy-terminal domain with multiple connections. *Exp. Mol. Med. 39*, 247–254.
5. de Almeida, S. F., and Carmo-Fonseca, M. (2008) The CTD role in cotranscriptional RNA processing and surveillance. *FEBS Lett. 582*, 1971–1976.
6. Allison, L. A., Moyle, M., Shales, M., and Ingles, C. J. (1985) Extensive homology among the large subunits of eukaryotic and prokaryotic RNA polymerases. *Cell 42*, 599–610.
7. Corden, J. L., Cadena, D. L., Ahearn, J. M., and Dahmus, M. E. (1985) A unique structure at the carboxyl terminus of the largest subunit of eukaryotic RNA polymerase II. *Proc. Natl. Acad. Sci. U.S.A. 82*, 7934–7938.
8. Cadena, D. L., and Dahmus, M. E. (1987) Messenger RNA synthesis in mammalian cells is catalyzed by the phosphorylated form of RNA polymerase II. *J. Biol. Chem. 262*, 12468–12474.
9. Lu, H., Flores, O., Weinmann, R., and Reinberg, D. (1991) The nonphosphorylated form of the RNA polymerase II preferentially associates with the preinitiation complex. *Proc. Natl. Acad. Sci. U.S.A. 88*, 10004–10008.
10. O'Brien, T. S., Hardin, S., Greenleaf, A., and Lis, J. T. (1994) Phosphorylation of RNA polymerase II C-terminal domain and transcriptional elongation. *Nature 370*, 75–77.
11. Dahmus, M. E. (1996) Reversible phosphorylation of the C-terminal domain of RNA polymerase II. *J. Biol. Chem. 271*, 19009–19012.
12. Cho, H., Kim, T. K., Mancebo, H., Lane, W. S., Flores, O., and Reinberg, D. (1999) A protein phosphatase functions to recycle RNA polymerase II. *Genes Dev. 13*, 1540–1552.
13. Chambers, R. S., and Dahmus, M. E. (1994) Purification and characterization of a phosphatase from HeLa cells which dephosphorylates the C-terminal domain of RNA polymerase II. *J. Biol. Chem. 269*, 26243–26248.
14. Chambers, R. S., and Dahmus, M. E. (1996) Purification and characterization of an RNA polymerase II phosphatase from yeast. *J. Biol. Chem. 271*, 24498–24504.
15. Archambault, J., Pan, G., Dahmus, G. K., Cartier, M., Marshall, N., Zhang, S., Dahmus, M. E., and Greenblatt, J. (1998) FCP1, the RAP74-interacting subunit of a human protein phosphatase that dephosphorylates the carboxy-terminal domain of RNA polymerase IIO. *J. Biol. Chem. 273*, 27593–27601.
16. Kobor, M. S., Archambault, J., Lester, W., Holstege, F. C. P., Gileadi, O., Jansma, D. B., Jennings, E. G., Kouyoumdjian, F., Davidson, A. R., Young, R. A., et al. (1999) An unusual eukaryotic protein phosphatase required for transcription by RNA polymerase II and CTD dephosphorylation in *S. cerevisiae*. *Mol. Cell 4*, 55–62.
17. Kimura, M., Suzuki, H., and Ishihama, A. (2002) Formation of a carboxy-terminal domain phosphatase (Fcp1)/TFIIF/RNA polymerase II (pol II) complex in *Schizosaccharomyces pombe* involves direct interaction between Fcp1 and the Rpb4 subunit of pol II. *Mol. Cell. Biol. 22*, 1577–1588.
18. Jeronimo, C., Langelier, M. F., Zeghouf, M., Cojocaru, M., Bergeron, D., Baali, D., Forget, D., Mnaimneh, S., Davierwala, A. P., Pootoolal, J., et al. (2004) RPAP1, a novel human RNA polymerase II-associated protein affinity purified with recombinant wild-type and mutated polymerase subunits. *Mol. Cell. Biol. 24*, 7043–7058.
19. Cho, E.-J., Kobor, M. S., Kim, M., Greenblatt, J., and Buratowski, S. (2001) Opposing effects of Ctk1 kinase and Fcp1 phosphatase at Ser 2 of the RNA polymerase II C-terminal domain. *Genes Dev. 15*, 3319–3329.
20. Hausmann, S., and Shuman, S. (2002) Characterization of the CTD phosphatase Fcp1 from fission yeast. Preferential dephosphorylation of serine 2 versus serine 5. *J. Biol. Chem. 277*, 21213–21220.
21. Mandal, S. S., Cho, H., Kim, S., Cabane, K., and Reinberg, D. (2002) FCP1, a phosphatase specific for the heptapeptide repeat of the largest subunit of RNA polymerase II, stimulates transcription elongation. *Mol. Cell. Biol. 22*, 7543–7552.
22. Abbott, K. L., Archambault, J., Xiao, H., Nguyen, B. D., Roeder, R. G., Greenblatt, J., Omichinski, J. G., and Legault, P. (2005) Interactions of the HIV-1 Tat and RAP74 proteins with the RNA polymerase II CTD phosphatase FCP1. *Biochemistry 44*, 2716–2731.
23. Chambers, R. S., Wang, B. Q., Burton, Z. F., and Dahmus, M. E. (1995) The activity of COOH-terminal domain phosphatase is regulated by a docking site on RNA polymerase II and by the general transcription factors IIF and IIB. *J. Biol. Chem. 270*, 14962–14969.
24. Flores, O., Maldonado, E., Burton, Z., Greenblatt, J., and Reinberg, D. (1988) Factors involved in specific transcription by mammalian RNA polymerase II. RNA polymerase II-associating protein 30 is an essential component of transcription factor IIF. *J. Biol. Chem. 263*, 10812–10816.
25. Flores, O., Ha, I., and Reinberg, D. (1990) Factors involved in specific transcription by mammalian RNA polymerase II. Purification and subunit composition of transcription factor IIF. *J. Biol. Chem. 265*, 5629–5634.
26. Finkelstein, A., Kostrub, C. F., Li, J., Chavez, D. P., Wang, B. Q., Fang, S. M., Greenblatt, J., and Burton, Z. F. (1992) A cDNA encoding RAP74, a general initiation factor for transcription by RNA polymerase II. *Nature 355*, 464–467.

27. Fang, S. M., and Burton, Z. F. (1996) RNA polymerase II-associated protein (RAP) 74 binds transcription factor (TF) IIB and blocks TFIIB-RAP30 binding. *J. Biol. Chem. 271*, 11700–11709.
28. Wang, B. Q., and Burton, Z. F. (1995) Functional domains of human RAP74 including a masked polymerase binding domain. *J. Biol. Chem. 270*, 27035–27044.
29. Tan, S., Conaway, R. C., and Conaway, J. W. (1995) Dissection of transcription factor TFIIF functional domains required for initiation and elongation. *Proc. Natl. Acad. Sci. U.S.A. 92*, 6042–6046.
30. Archambault, J., Chambers, R. S., Kobor, M. S., Ho, Y., Cartier, M., Bolotin, D., Andrews, B., Kane, C. M., and Greenblatt, J. (1997) An essential component of a C-terminal domain phosphatase that interacts with transcription factor IIF in *Saccharomyces cerevisiae*. *Proc. Natl. Acad. Sci. U.S.A. 94*, 14300–14305.
31. Kobor, M. S., Simon, L. D., Omichinski, J., Zhong, G., Archambault, J., and Greenblatt, J. (2000) A motif shared by TFIIF and TFIIB mediates their interaction with the RNA polymerase II carboxy-terminal domain phosphatase Fcp1p in *Saccharomyces cerevisiae*. *Mol. Cell. Biol. 20*, 7438–7449.
32. Nguyen, B. D., Chen, H.-T., Kobor, M. S., Greenblatt, J., Legault, P., and Omichinski, J. G. (2003) Solution structure of the carboxyl-terminal domain of RAP74 and NMR characterization of the FCP1-binding sites of RAP74 and human TFIIB. *Biochemistry 42*, 1460–1469.
33. Nguyen, B. D., Abbott, K. L., Potempa, K., Kobor, M. S., Archambault, J., Greenblatt, J., Legault, P., and Omichinski, J. G. (2003) NMR structure of a complex containing the TFIIF subunit RAP74 and the RNA polymerase II carboxyl-terminal domain phosphatase FCP1. *Proc. Natl. Acad. Sci. U.S.A. 100*, 5688–5693.
34. Palancade, B., Dubois, M.-F., and Bensaude, O. (2002) FCP1 phosphorylation by casein kinase 2 enhances binding to TFIIF and RNA polymerase II carboxyl-terminal domain phosphatase activity. *J. Biol. Chem. 277*, 36061–36067.
35. Friedl, E. M., Lane, W. S., Erdjument-Bromage, H., Tempst, P., and Reinberg, D. (2003) The C-terminal domain phosphatase and transcription elongation activities of FCP1 are regulated by phosphorylation. *Proc. Natl. Acad. Sci. U.S.A. 100*, 2328–2333.
36. Abbott, K. L., Renfrow, M. B., Chalmers, M. J., Nguyen, B. D., Marshall, A. G., Legault, P., and Omichinski, J. G. (2005) Enhanced binding of RNAP II CTD phosphatase FCP1 to RAP74 following CK2 phosphorylation. *Biochemistry 44*, 2732–2745.
37. Kamada, K., De Angelis, J., Roeder, R. G., and Burley, S. K. (2001) Crystal structure of the C-terminal domain of the RAP74 subunit of human transcription factor IIF. *Proc. Natl. Acad. Sci. U.S.A. 98*, 3115–3120.
38. Kamada, K., Roeder, R. G., and Burley, S. K. (2003) Molecular mechanism of recruitment of TFIIF-associating RNA polymerase C-terminal domain phosphatase (FCP1) by transcription factor IIF. *Proc. Natl. Acad. Sci. U.S.A. 100*, 2296–2299.
39. Kay, L. E., Keifer, P., and Saarinen, T. (1992) Pure absorption gradient enhanced heteronuclear single quantum correlation spectroscopy with improved sensitivity. *J. Am. Chem. Soc. 114*, 10663–10665.
40. Wider, G., Weber, C., Traber, R., Widmer, H., and Wüthrich, K. (1990) Use of a double-half-filter in two-dimensional ^{1}H nuclear magnetic resonance studies of receptor-bound cyclosporin. *J. Am. Chem. Soc. 112*, 9015–9016.
41. Vuister, G. W., and Bax, A. (1992) Resolution enhancement and spectral editing of uniformly ^{13}C-enriched proteins by homonuclear broadband ^{13}C decoupling. *J. Magn. Reson. 98*, 428–435.
42. Santoro, J., and King, G. C. (1992) A constant-time 2D overbodenhausen experiment for inverse correlation of isotopically enriched species. *J. Magn. Reson. 97*, 202–207.
43. Vuister, G. W., and Bax, A. (1993) Quantitative J correlation: A new approach for measuring homonuclear three-bond J (H^NH^α) coupling constants in ^{15}N-enriched proteins. *J. Am. Chem. Soc. 115*, 7772–7777.
44. Kuboniwa, H., Grzesiek, S., Delaglio, F., and Bax, A. (1994) Measurement of HN-Hα J couplings in calcium-free calmodulin using new 2D and 3D water-flip-back methods. *J. Biomol. NMR 4*, 871–878.
45. Wittekind, M., and Mueller, L. (1993) HNCACB, a high-sensitivity 3D NMR experiment to correlate amide-proton and nitrogen resonances with the α- and β-carbon resonances in proteins. *J. Magn. Reson., Ser. B,* 201–205.
46. Grzesiek, S., Dobeli, H., Gentz, R., Garotta, G., Labhardt, A. M., and Bax, A. (1992) ^{1}H, ^{13}C, and ^{15}N NMR backbone assignments and secondary structure of human interferon-γ. *Biochemistry 31*, 8180–8190.
47. Muhandiram, D. R., and Kay, L. E. (1994) Gradient-enhanced triple-resonance three-dimensional NMR experiments with improved sensitivity. *J. Magn. Reson., Ser. B 103*, 203–216.
48. Grzesiek, S., Ikura, M., Clore, G. M., Gronenborn, A. M., and Bax, A. (1992) A 3D triple-resonance NMR technique for qualitative measurement of carbonyl-Hb J couplings in isotopically enriched proteins. *J. Magn. Reson. 96*, 215–221.
49. Grzesiek, S., Anglister, J., and Bax, A. (1993) Correlation of backbone amide and aliphatic side-chain resonances in ^{13}C/^{15}N-enriched proteins by isotropic mixing of ^{13}C magnetization. *J. Magn. Reson. 101*, 114–121.
50. Ikura, M., Kay, L. E., and Bax, A. (1991) Improved three-dimensional ^{1}H-^{13}C-^{1}H correlation spectroscopy of a ^{13}C-labeled protein using constant-time evolution. *J. Biomol. NMR 1*, 299–304.
51. Kay, L. E., Xu, G.-Y., Singer, A. U., Muhandiram, D. R., and Forman-Kay, J. D. (1993) A gradient-enhanced HCCH-TOCSY experiment for recording side chain ^{1}H and ^{13}C correlations in H_2O samples of proteins. *J. Magn. Reson., Ser. B 101*, 333–337.
52. Yamazaki, T., Forman-Kay, J. D., and Kay, L. E. (1993) Two-dimensional NMR experiments for correlating $^{13}C\beta$ and $^1H\delta/\varepsilon$ chemical shifts of aromatic residues in ^{13}C-labeled proteins via scalar couplings. *J. Am. Chem. Soc. 115*, 11054–11055.
53. Zhang, O., Kay, L. E., Olivier, J. P., and Forman-Kay, J. D. (1994) Backbone ^{1}H and ^{15}N resonance assignments of the N-terminal SH3 domain of drk in folded and unfolded states using enhanced-sensitivity pulsed field gradient NMR techniques. *J. Biomol. NMR 4*, 845–858.
54. Marion, D., Kay, L. E., Sparks, S. W., Torchia, D. A., and Bax, A. (1989) Three-dimensional NMR of ^{15}N-labeled proteins. *J. Am. Chem. Soc. 111*, 1515–1517.
55. Zuiderweg, E. R. P., McIntosh, L. P., Dahlquist, F. W., and Fesik, S. W. (1990) Three-dimensional carbon-13-resolved proton NOE spectroscopy of uniformly carbon-13-labeled proteins for the NMR assignment and structure determination of larger molecules. *J. Magn. Reson. 86*, 210–216.
56. Zwahlen, C., Legault, P., Vincent, S. J. F., Greenblatt, J., Konrat, R., and Kay, L. E. (1997) Methods for measurement of intermolecular NOEs by multinuclear NMR spectroscopy: Application to a bacteriophage lambda N-peptide/*box*B RNA. *J. Am. Chem. Soc. 119*, 6711–6721.
57. Delaglio, F., Grzesiek, S., Vuister, G. W., Zhu, G., Pfeifer, J., and Bax, A. (1995) NMRPipe: A multidimensional spectral processing system based on UNIX pipes. *J. Biomol. NMR 6*, 277–293.
58. Johnson, B. A., and Blevins, R. A. (1994) NMRView: A computer program for the visualization and analysis of NMR data. *J. Biomol. NMR 4*, 603–614.
59. Cornilescu, G., Delaglio, F., and Bax, A. (1999) Protein backbone angle restraints from searching a database for chemical shift and sequence homology. *J. Biomol. NMR 13*, 289–302.
60. Brunger, A. T., Adams, P. D., Clore, G. M., Gros, P., Grosse-Kunstleve, R. W., Jiang, J.-S., Kuszewski, J., Nilges, M., Pannu, N. S., Read, R. J., et al. (1998) Crystallography and NMR system (CNS): A new software system for macromolecular structure determination. *Acta Crystallogr. D54*, 905–921.
61. Kleywegt, G. T., and Jones, T. A. (1998) Databases in protein crystallography. *Acta Crystallogr. D54*, 1119–1131.
62. Kuszewski, J., Gronenborn, A. M., and Clore, G. M. (1996) Improving the quality of NMR and crystallographic protein structures by means of a conformational database potential derived from structure databases. *Protein Sci. 5*, 1067–1080.
63. Laskowski, R. A., Antoon, J., Rullmann, C., Macarthur, M. W., Kaptein, R., and Thornton, J. M. (1996) AQUA and PROCHECK-NMR: Programs for checking the quality of protein structures solved by NMR. *J. Biomol. NMR 8*, 477–486.
64. DeLano, W. L. (2002) The PyMOL molecular graphics system, DeLano Scientific, San Carlos, CA.
65. Pace, C. N., Vajdos, F., Fee, L., Grimsley, G., and Gray, T. (1995) How to measure and predict the molar absorption coefficient of a protein. *Protein Sci. 4*, 2411–2423.
66. Turnbull, W. B., and Daranas, A. H. (2003) On the value of c: Can low affinity systems be studied by isothermal titration calorimetry. *J. Am. Chem. Soc. 125*, 14859–14866.
67. Di Lello, P., Jenkins, L. M., Jones, T. N., Nguyen, B. D., Hara, T., Yamaguchi, H., Dikeakos, J. D., Appella, E., Legault, P., and Omichinski, J. G. (2006) Structure of the Tfb1/p53 complex:

Insights into the interaction between the p62/Tfb1 subunit of TFIIH and the activation domain of p53. *Mol. Cell 22*, 731–740.
68. Langlois, C., Mas, C., Di Lello, P., Jenkins, L. M., Legault, P., and Omichinski, J. G. (2008) NMR structure of the complex between the Tfb1 subunit of TFIIH and the activation domain of VP16: Structural similarities between VP16 and p53. *J. Am. Chem. Soc. 130*, 10596–10604.
69. Robert, F., Douziech, M., Forget, D., Egly, J. M., Greenblatt, J., Burton, Z. F., and Coulombe, B. (1998) Wrapping of promoter DNA around the RNA polymerase II initiation complex induced by TFIIF. *Mol. Cell 2*, 341–351.
70. Varon, R., Gooding, R., Steglich, C., Marns, L., Tang, H., Angelicheva, D., Yong, K. K., Ambrugger, P., Reinhold, A., Morar, B., et al. (2003) Partial deficiency of the C-terminal-domain phosphatase of RNA polymerase II is associated with congenital cataracts facial dysmorphism neuropathy syndrome. *Nat. Genet. 35*, 185–189.
71. Kamenski, T., Heilmeier, S., Meinhart, A., and Cramer, P. (2004) Structure and mechanism of RNA polymerase II CTD phosphatases. *Mol. Cell 15*, 399–407.

BI801549M